

PAPER • OPEN ACCESS

Evaluation of the VDA 238-100 Tight Radius Bending Test using Digital Image Correlation Strain Measurement

To cite this article: K Cheong et al 2017 J. Phys.: Conf. Ser. 896 012075

View the article online for updates and enhancements.

You may also like

- ESTIMATION OF THE RELEASE TIME OF SOLAR ENERGETIC PARTICLES NEAR THE SUN Yang Wang and Gang Qin
- Secure authentication and encryption via diffraction imaging-based encoding and vector decomposition
- Zhenyu Zhang, Sheng Wang, Shangying Zhou et al.
- COSMIC EVOLUTION OF DUST IN GALAXIES: METHODS AND PRELIMINARY RESULTS Kenji Bekki



doi:10.1088/1742-6596/896/1/012075

Evaluation of the VDA 238-100 Tight Radius Bending Test using Digital Image Correlation Strain Measurement

K Cheong¹, K Omer¹, C Butcher¹, R George¹ and J Dykeman²

K Cheong: dwkcheon@uwaterloo.ca, K Omer: komer@uwaterloo.ca, C Butcher: cbutcher@uwaterloo.ca, R George: ryan.george@uwaterloo.ca, J Dykeman: jdykeman@oh.hra.com

Abstract. The VDA238-100 standard for tight radius bending (v-bending) of sheet materials has received widespread acceptance with automotive suppliers and material producers to characterize local formability. However, the test fixture and tooling in the v-bend test standard is not amenable to direct strain measurement and the operator cannot terminate the test at the onset of crack initiation as the outer bend surface is not visible. Consequently, fracture is identified using a load threshold and the bend angle estimated from an analytical formula based upon the punch displacement and tooling geometry. Bend angles are not directly transferable and must be interpreted relative to the sheet thickness and bend radius unlike a strain measurement. By obtaining an in-situ strain measurement on the surface using digital image correlation (DIC), the plane strain fracture limit can be accurately identified at the onset of cracking and remove ambiguity in translating the bend angles to practical forming operations and simulations. A novel inverted VDA test frame was developed to incorporate DIC strain measurement during the bend test and a variety of advanced high strength sheet materials were evaluated. It was observed that the VDA bend test creates a homogeneous strain state of plane strain across the width of the sample along with a proportional strain path to fracture without necking that is ideal for fracture characterization. A correlation is developed to relate the bend angle with the major strain for the materials considered and accounts for the sheet thickness and bend radius. A comparison of the bend angle obtained using the formula in the VDA standard based on the punch displacement was in very good agreement with manual measurements and an algorithm to measure the bend angle using DIC analysis was developed.

1. Introduction

With the rapid development and adoption of advanced high strength steel and aluminium alloys for vehicle lightweighting, the material bendability has emerged as a critical performance metric. In the forming of sheet materials, bending creates a plane strain loading condition as the sheet is usually very wide and thin relative to the bend radius of the tooling. Similarly, during an automotive crash event, structural components such as a crush rail will fold and bend where severe tight radius bending occurs within the folding regions. In tight radius bending as found in folds, the strain state is one of plane

¹ Department Mechanical and Mechatronics Engineering, University of Waterloo, 200 University Ave W., Waterloo ON, N2L 3G1, Canada

² Honda R&D Americas Inc., 21001 State Route 739, Raymond, Ohio, United States, 43067-9705

doi:10.1088/1742-6596/896/1/012075

strain tension that also corresponds to the lowest ductility of sheet materials. As such, the bendability (usually characterized using a bend angle) provides critical insight into the plane strain fracture limit.

The shift towards plane strain characterization using a tight radius bend test rather than the long established methods involving forming limit curves (FLCs) is due to the mechanics of bending that can mitigate necking instabilities. The plane strain loading condition associated with a Nakazima test for FLC determination is one of tensile stretching with minimal bending due to the large punch radius. This leads to a relatively homogeneous stretching mode through the thickness of the sheet that promotes the development of a neck (instability) leading to strain localization and fracture. Conversely, in a tight radius bending operation, the loading is also plane strain but with a strong strain gradient from plane strain tension at the outer radius of the bend and plane strain compression at the inner bend that is in contact with the punch. The strong strain gradient and shifting of the neutral axis with deformation can thus lead to cracking of the outer material fibres in plane strain tension before the onset of a necking instability [1]. The transition between the two types of failure modes can be investigated using stretch-bending tests as discussed in Tharrett and Stoughton [2] by altering the ratio of the sheet thickness to punch radius (t/R). Without the complications associated with necking, the bendability provides a more direct measure of the material performance in plane strain.

In contrast to stretch-bending tests, the VDA 238-100 test standard was developed for pure bending and is essentially a three-point bend test with a sharp punch radius and minimal spacing between the bend supports. Requirements are standardized punch tip radius, roller spacing, sample width, sample thickness, and roller radius [3]. A convenient analytical formula [3] is employed to estimate the bend angle based on the punch displacement when the load threshold is reached. The simplicity, consistency and detailed specifications on the tooling and test parameters are the strength of the VDA standard that has led to its widespread acceptance.

Unfortunately, the relatively simple setup is only capable of providing limited data: punch load and displacement. The bend angle can be estimated by analytical formulas but highly theoretical. Furthermore, the bend angle at fracture is not directly transferable into numerical models to predict fracture as it is not a strain measurement. To address these limitations in the VDA test standard, a novel test frame was developed to enable *in-situ* strain measurement using digital image correlation (DIC).

2. Experimental set up

The basic concept in designing a VDA compatible bend test with stereographic DIC is to invert the test so that the punch remains stationary and the rollers move downwards to perform the bending. The advantage of this re-configuration is two-fold: (1) DIC cameras can be easily positioned to view the outer bend and (2) the stationary punch ensures that the viewing area of the DIC does not move out of plane so that DIC strain resolution is not compromised. To permit an enhanced viewing area for the DIC (Figure 1), the rollers are chamfered at 65° which leaves sufficient arc length of the rollers to perform a 180° bend with typical blank sizes before the chamfered section is reached. Figure 2 shows a cross-section view of the model perpendicular to the punch knife; (A): parallel rollers, (B): punch stroke part (move down), (C): specimen, and (D): fixed punch (knife).

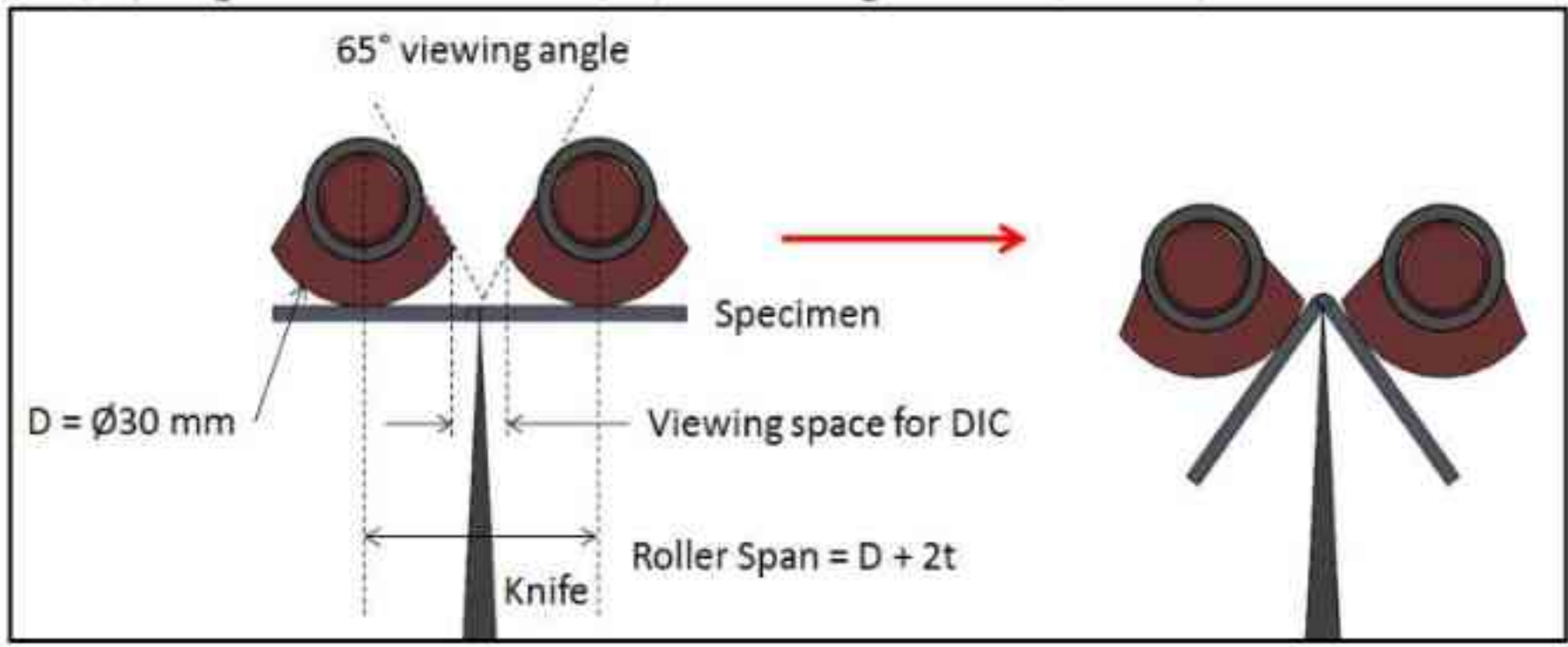


Fig. 1 Concept for the tight radius three-point bending process with DIC strain measurement

doi:10.1088/1742-6596/896/1/012075

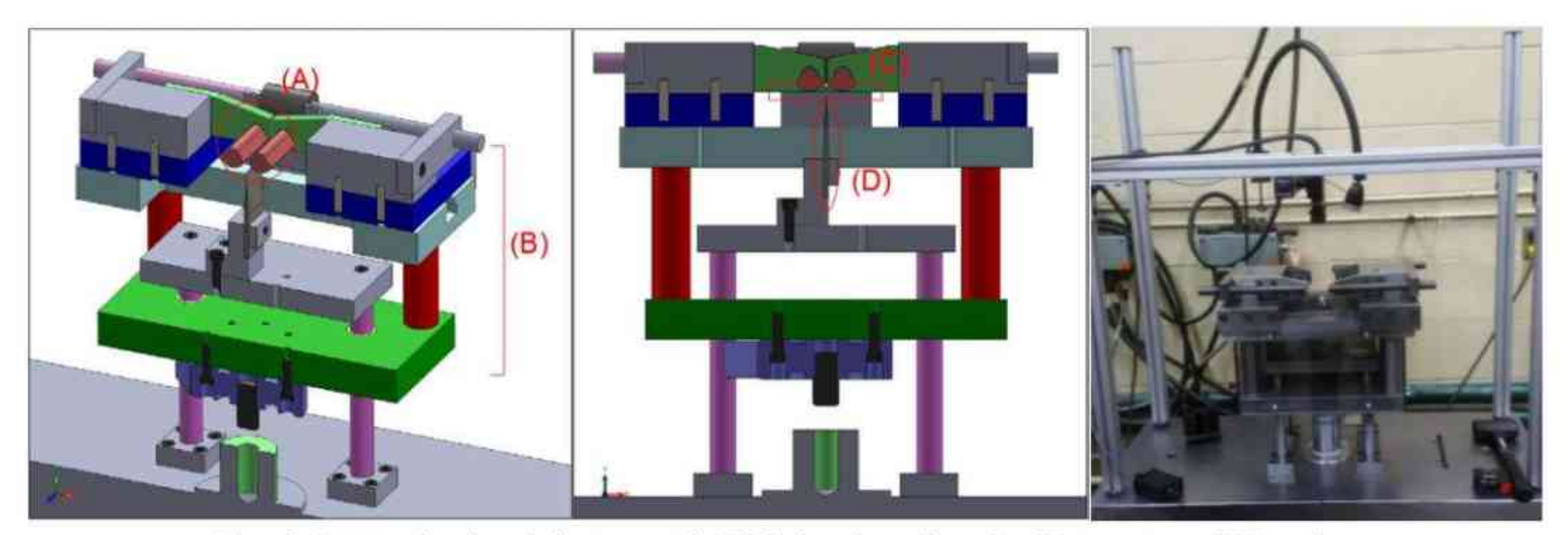


Fig. 2 Inverted v-bend device with DIC developed at the University of Waterloo

For a specimen width of 50 mm, the DIC resolution of the entire width of the bend is 0.02 mm/pixel which can be increased if a smaller specimen width is used as the camera position is adjustable. The VDA 238-100 criterion states minimum of 20x the thickness samples could be used for many sheet metals. The DIC strain analysis was performed using VIC-7 software from Correlated Solutions Inc. In this study, the settings employed in the DIC analysis was a subset ranging from 29-45, a step size of 5 and a strain filter size of 5 pixels that correspond to an approximate virtual strain gauge length of 0.5 mm [4]. A frame rate of 10 frames per second was observed to be sufficient to capture the onset of cracking during the test with a punch velocity of 20 mm/min. A punch with a nominal tip radius of 0.40 mm was employed with an as-fabricated tip radius of 0.43 mm. The roller spacing was adjusted based on sheet thickness in accordance with the VDA [3]. To avoid the potential for edge cracking, the specimens were fabricated using a machined edge using either CNC or EDM.

A total of 17 different specimen conditions of various strengths and ductility were considered and are listed in Table 1. A wide range of advanced high strength steel (AHSS) was considered with an addition of a variety of ultra-high strength steel (UHSS) with different thermal processes that correspond to in-die heating conditions [5]. AA5182, a widely-used automotive aluminum alloy, and a rare-earth magnesium alloy, ZEK100, were also included to represent automotive non-ferrous alloys.

Material	Thickness	Direction	NOTE:
DP600	1.5	RD	
DP980	1.2/1.6/1.4	RD/TD	DQ: Die quenched
Trip780	1.5	RD	AC: Air cooled
Usibor400_DQ	1.25	RD	OQ: Oil quenched
Usibor1500_DQ	1.22	RD	WQ: Water quenched
Usibor1500_AC	1.22	RD	RD: Rolling direction
Usibor1500_OQ	1.22	RD	TD: Transverse direction
Usibor1500_WQ	1.22	RD	DD: Diagonal direction
AA5182-O	1.5	RD	n . n .:
ZEK100-O	1.5	RD/TD/DD	Punch Radius = 0.43 mm

Table 1 Specimen types (total of 17 conditions)

3. DIC Strain Measurement and Analysis

The initial and deformed area of interest (AOI) in the DIC is shown in Figure 3 and corresponds to the outer bend surface. Due to the homogeneous strain distribution across the width of the sample and that multiple cracks may form near simultaneous along the specimen width, the strains are extracted using a set of 5 line slices as done for forming limit detection in the ISO-12004-2 standard. Each line slice consists of 200 points that creates a strain distribution across the bend as shown in Figure 4. Approximated length of line slices can be estimated with viewing space which is dependent on sample

doi:10.1088/1742-6596/896/1/012075

thickness; 2 mm thick sample has a viewing space of 8 mm, see Figure 1. The time history of each line slice is analyzed using a custom Matlab® subroutine and averaged so that the reported failure strain for each test specimen consists of the peak strain at five locations along the width. As seen in Figure 4, the strain distributions are very uniform and this behaviour was observed in all of the materials tested.

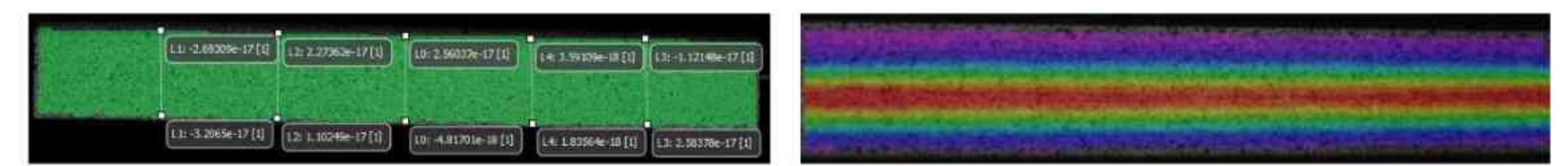


Fig. 3 Initial (left) and deformed AOI (right) of a DP980 steel at the image corresponding to the VDA load threshold with the sample width of 50 mm

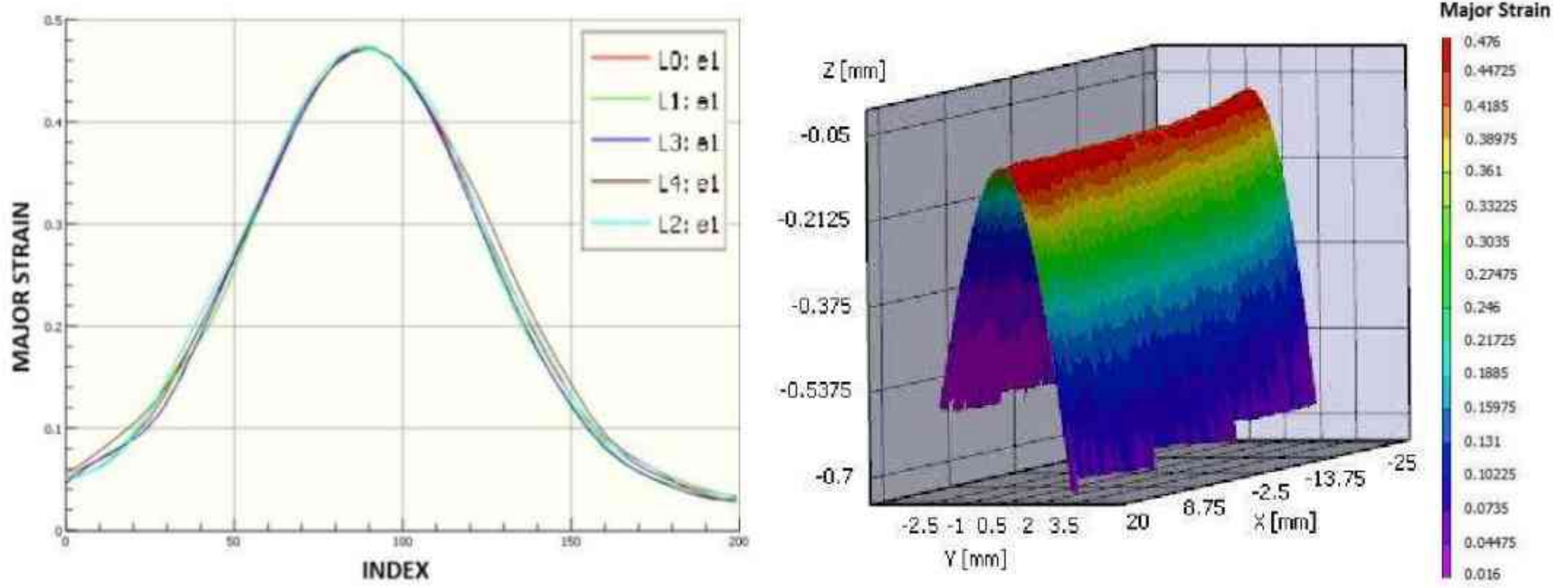


Fig. 4 Major true strain distribution for five line slices (left) and corresponding 3-D visualization (right) of a DP980 steel tested in the rolling direction at the image when the VDA load threshold was met

3.1. Fracture Identification

In a tight radius bending, fracture happens gradually in plane strain condition without "instant failure" due to the absence of necking. Thus, identifying the beginning and the last moment of fracture is ambiguous. The VDA standard suggests that the failure moment can be estimated using a 30 N or 60 N reduction from the peak load. For a sample less than 2 mm thickness, a load drop of 30 N is used while 60 N is used for thicker materials [2]. Note that this criterion is independent of the strength of the material so that a 1500 MPa strength UHSS with a sheet thickness of 1.2 mm would be evaluated using the same load threshold as a 500 MPa mild steel of the same thickness.

To investigate this definition of fracture, a visual inspection was performed using the recorded DIC images. Visual crack detection methods are subjective so upper and lower bound thresholds were established. The lower bound was defined as first initiation of a crack longer than 20 pixels which corresponds to 0.4 mm (Figure 5). This value was selected as a cut-off to distinguish between degradation of the painted speckle pattern and actual cracking. The upper bound limit was more subjective and corresponds to seeing a fracture surface emerge as in Figure 5 as the hair-line crack begins to open. Note that complete rupture of the specimen will occur past the upper bound and will be related to the crack resistance of the material.

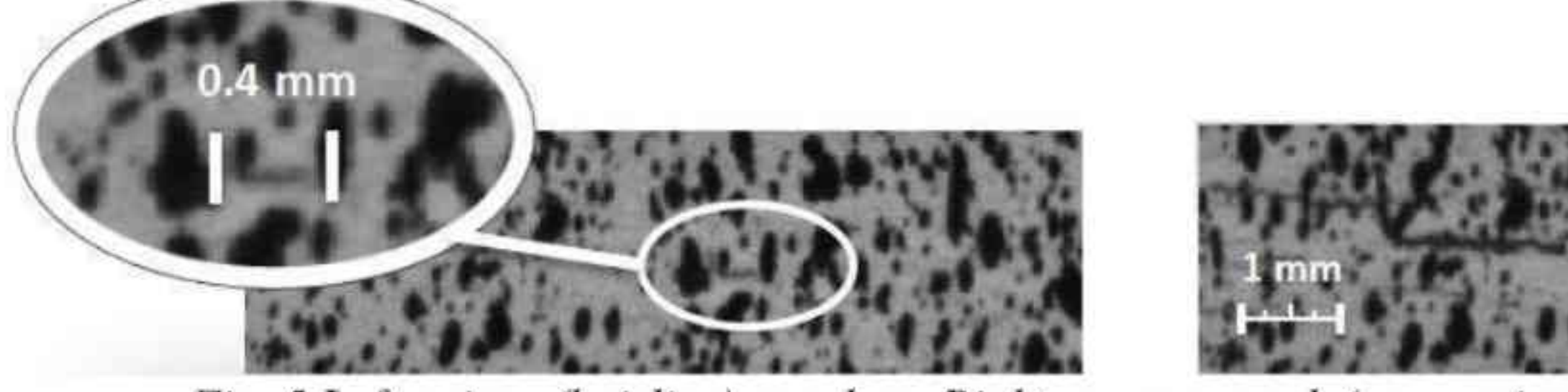


Fig. 5 Left: micro (hairline)-crack vs. Right: macro-crack (same orientation as Fig. 3)

Three DP980 steels were provided by different steel suppliers for the study. The sheet thicknesses of the materials were 1.2 mm, 1.4 mm, and 1.6 mm. These steels were tested in the rolling (RD) and transverse directions (TD) and the results are shown in Figure 6. The comparison between the visual lower bound, VDA criterion, and the visual upper bound shows that the overall, the VDA method appears to be a reasonable estimation at least for the three materials considered. The definition of cracking may also be dependent upon the desired application for the bend data. From a formability perspective, the onset of a hair line crack would denote a failed component as the surface has been compromised in which case the VDA estimate may be an upper bound. Conversely, from a crashworthiness perspective, complete cracking and rupture of the material might be preferred to identify the maximum amount of crash energy that can be absorbed by a structural component. In that case, the VDA criterion would likely constitute a lower bound estimate.

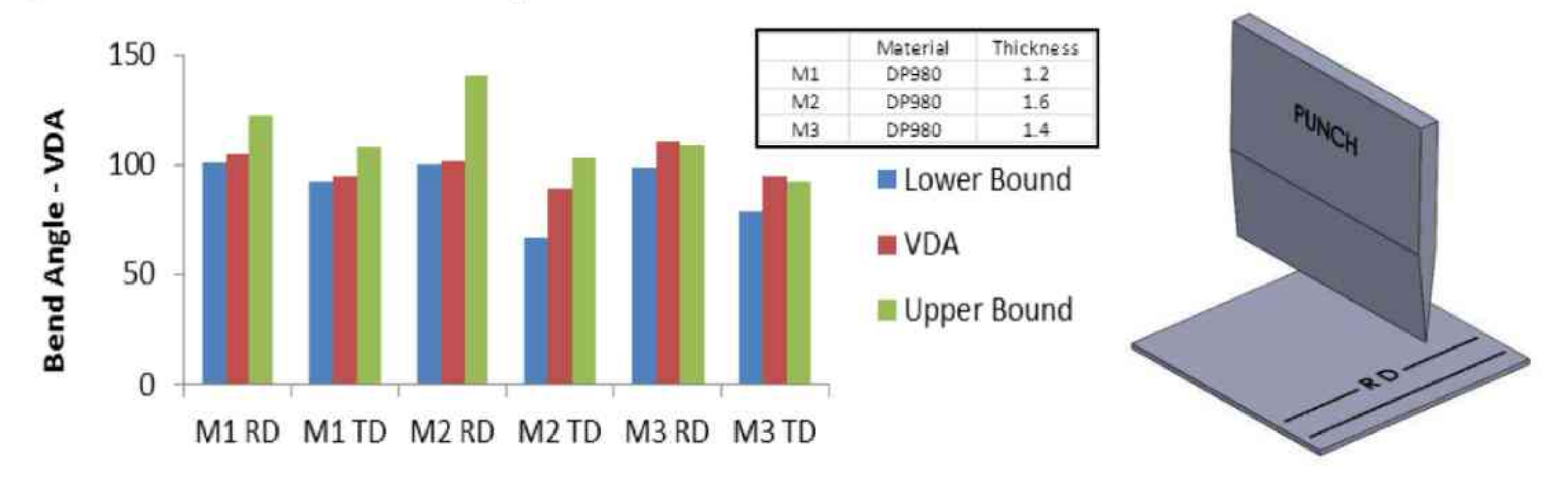


Fig. 6 Comparison of the Bend angle computed in Eq. (1) according to the punch displacement for three DP980 steels using the different fracture criteria (left). Rolling direction (RD) test setup (right)

4. Measurement of the Bend Angle

4.1. Theoretical bend angle from ISO and VDA standard

Analytical expressions for the bend angle, α , can be obtained based upon an idealized bending scenario from the roller radius, R, punch tip radius, r, roller gap, L, punch stroke, S, and the specimen thickness, a, as shown in Figure 7. The expressions for the bend angles in the respective ISO7438 (Eq. 1) and VDA 238-100 (Eq. 2) standards are given in reference [3][6][7]. The punch tip radius is not included in the VDA 238-100 bend angle formula but the punch tip radius is specified based upon the sheet thickness and material strength [3].

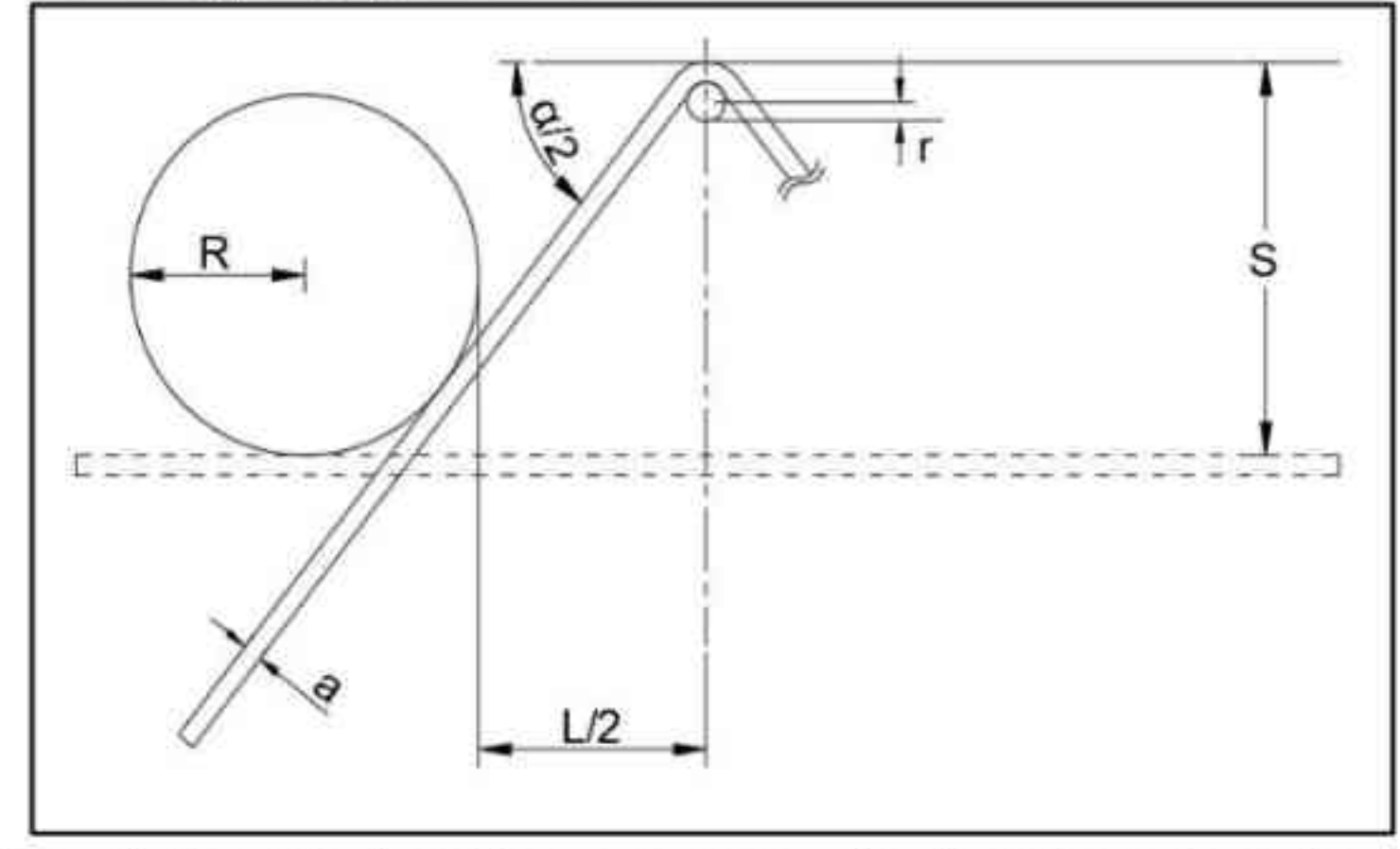


Fig. 7 Sample bending geometry for bend angle calculation

where:
$$\alpha^{VDA} = \alpha^{VDA} \left(R, a, L, S \right) \quad (1)$$

$$\alpha^{VDA} = 2 \left[-\tan^{-1} \left(\left(\frac{-h - \sqrt{h^2 - 4g \cdot i}}{2g} \right)^{-1} \sqrt{(R + a)^2 - \left(\left(\frac{-\sqrt{h^2 - 4g \cdot i} - h}}{2g} \right) + \left(R + \frac{L}{2} \right) \right)^2} - (R + a - S) \right] \cdot \frac{180^{\circ}}{\pi} \right]$$

doi:10.1088/1742-6596/896/1/012075

$$g = \left(R + \frac{L}{2}\right)^{2} + (R + a - S)^{2}$$

$$h = 2(R + a)^{2} \cdot \left(-\left(R + \frac{L}{2}\right)\right) + 2\left(R + \frac{L}{2}\right)^{3} - 2(R + a - S)^{2} \cdot \left(-\left(R + \frac{L}{2}\right)\right)$$

$$i = (R + a)^{4} - 2(R + a)^{2} \cdot \left(R + \frac{L}{2}\right)^{2} - (R + a - S)^{2} \cdot (R + a)^{2} + (R + a - S)^{2} \cdot \left(R + \frac{L}{2}\right)^{2} + \left(R + \frac{L}{2}\right)^{4}$$

$$\alpha^{ISO} = \alpha^{VAS - TKSE} = 2\left(\sin^{-1}\left(\frac{R + r + a}{\sqrt{(S - (R + r + a))^{2} + (R + L/2)^{2}}}\right) + \tan^{-1}\left(\frac{S - (R + r + a)}{R + L/2}\right)\right) \frac{180^{\circ}}{\pi}$$
(2)

Since the ISO and VDA approach of the bend angle rely on these analytical formulas, experimental errors are inevitable. Larour et al. [8] demonstrated the sensitivity of these formulae to factors such as the machine stiffness, sheet curvature, punch tip lift off, and roller shift. To revisit the comparison between the different bend angle definitions with the DIC test results, the bend angles at fracture for the 17 conditions of materials listed in Table 1 were manually measured. Measuring the angle of the samples that have exhibited partial surface cracking was to minimize the influence of springback on the measurements as cracking will relieve some of the internal stress. For consistency, the last image recorded by the DIC system was then analyzed as this coincided with the end of the test but before unloading of the specimen. The results are presented in Figure 8. Overall, for the 17 material conditions evaluated, the VDA bend angle in Eq. (1) performed slightly better than the ISO bend angle in Eq. (2) which tended to overestimate the bend angle. The preference for agreement with the VDA over the ISO bend angle may also be related to the machine stiffness and design of the inverted tooling. The adjusted coefficients of determination [9], R², were calculated to evaluate the linearity between the theoretical and measured bend angles with the VDA correlation obtaining an R² of 0.98, and the ISO correlation a value of 0.95.

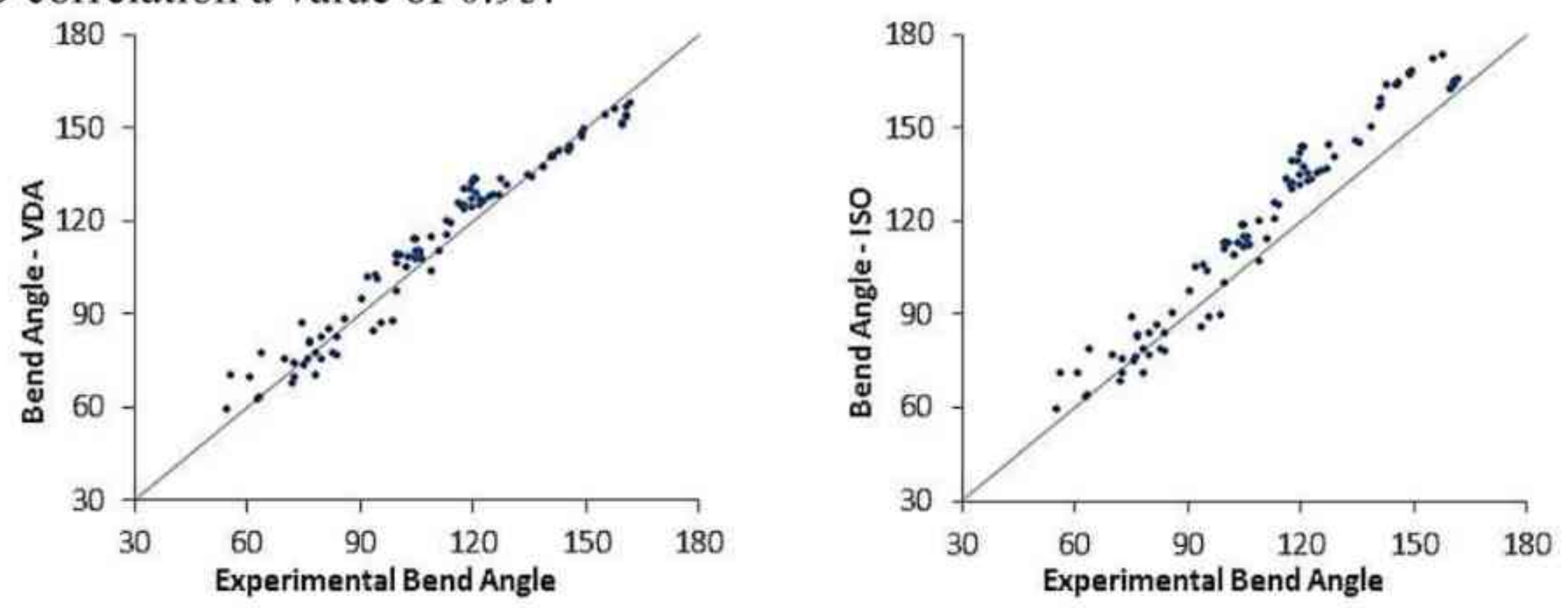


Fig. 8 Experimental vs. theoretical bend angle from VDA (left) and ISO (right)

4.2. Experimental bend angle from DIC measurement

Another representation of the bend angle can be obtained from the stereographic DIC data where the displacement of points can be tracked along the region of interest. Neuhaus et al. [10] have also investigated bend angle measurement using optical methods but without DIC. The bent specimen has round tip at the fracture location thus extension lines have to be drawn to evaluate the bend angle, see Figure 9. The automated measurement of the bend angle using this data is not straightforward as the specimen is rounded and only a portion of the bend is visible. To mimic the physical measurement method using a protractor, a best fit linear line was performed for each side of the bend and the intersection of the lines can define the bend angle. However, due to the rounding of the sample in the area of interest, a selection criterion is needed to identify the points that are sufficiently far enough away from the bend apex where the strain is highest. The proposed algorithm involves selecting the points based upon their relative strain level. If a point had a strain level of a specific threshold lower than the peak strain, it was included in the fitting region. The four threshold levels were 90%, 75%, 50% and 25% as their strain filters (percentage lower than threshold strain), see Figure 9.

doi:10.1088/1742-6596/896/1/012075

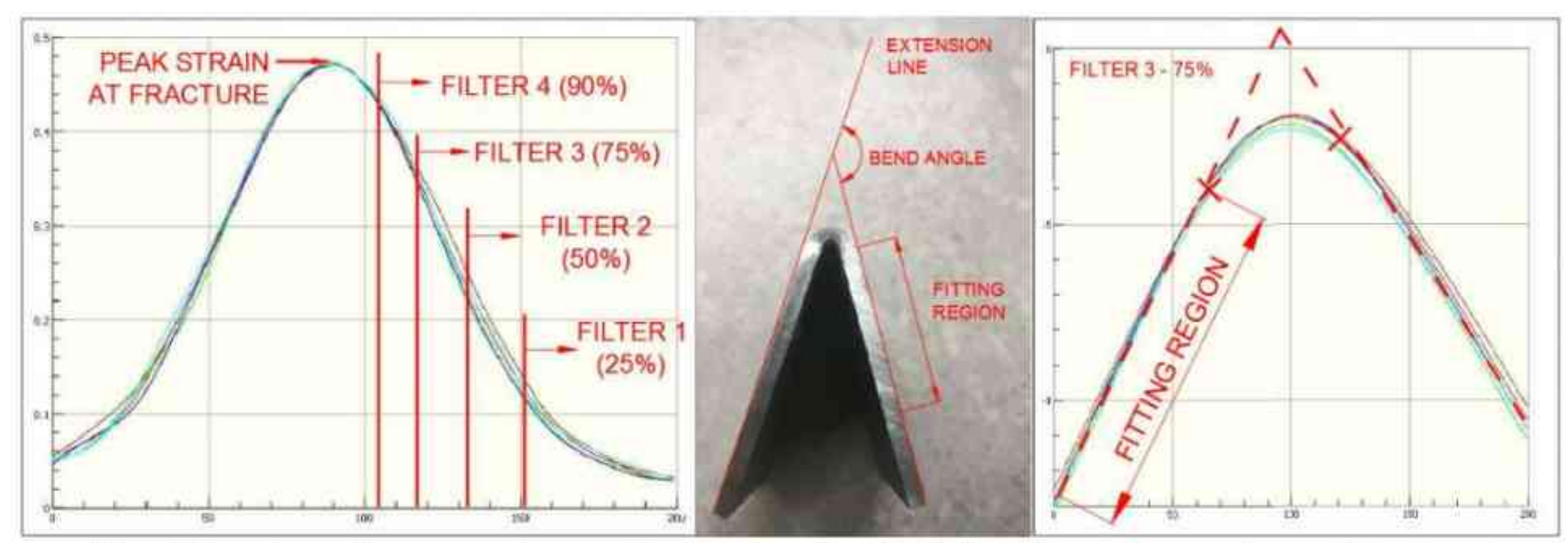


Fig. 9 Bend angle measuring method using the DIC data from the surface of the bend

As shown in Figure 10, the best results were obtained using the strain filter of 25% with the DIC measured bend angle being in decent agreement with the bend angle from the VDA correlation. An adjusted R² value of 0.90 was obtained but there is still room for improvement and the angle measurement algorithm will be revised in future work.

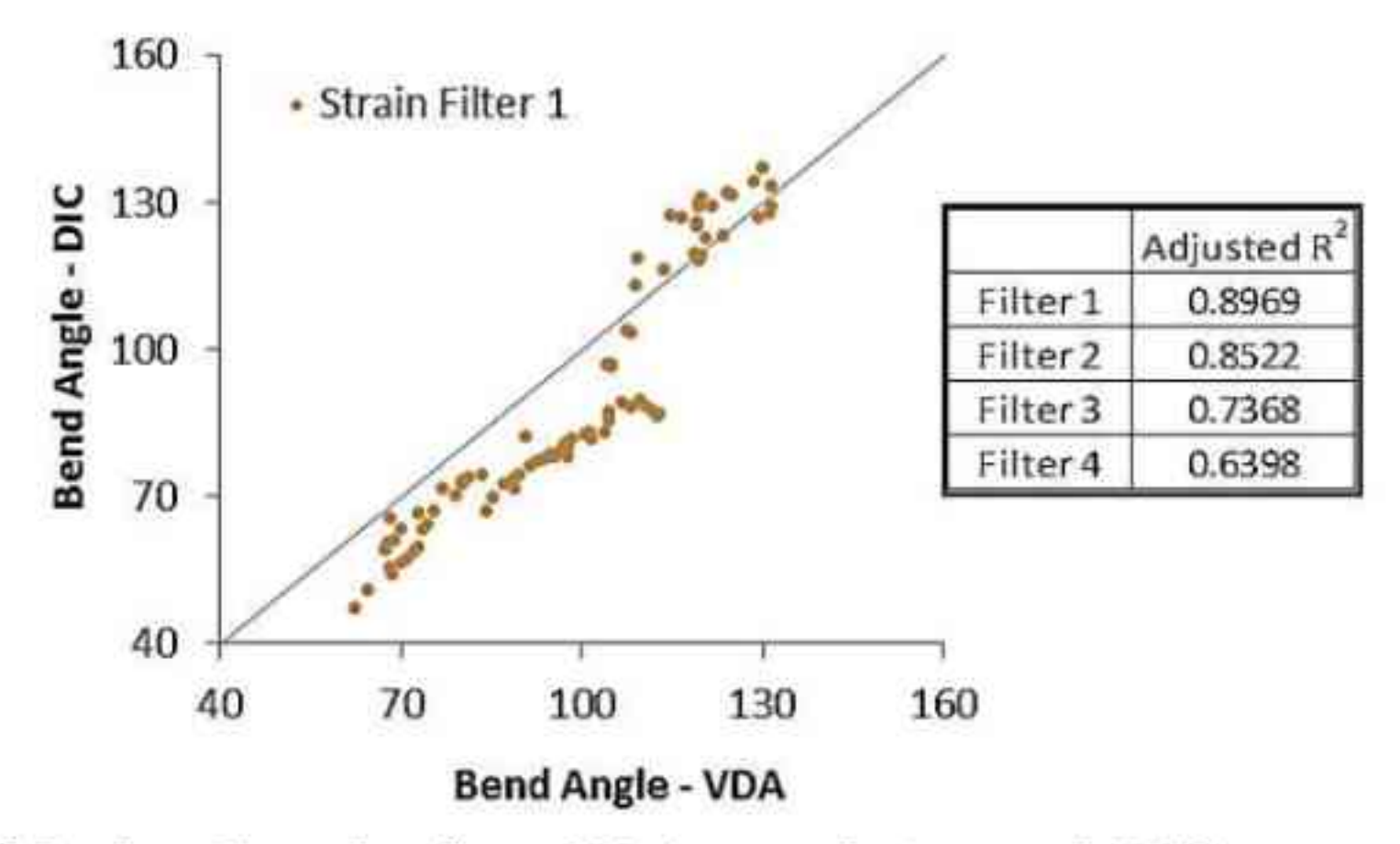


Fig. 10 Comparison of the bend angles from VDA correlation and DIC measurement with filter of 25%

5. Sensitivity Analysis regarding bend angle and major strain

Conventional forming operation often estimates the fracture limit using a load threshold and the bend angle. However, the bend angle is not always preferable due to its dependence on the sheet thickness and the bend radius unlike a strain measurement. Therefore with the addition of the DIC system, it is important to understand the relationship between the bend angle and the major strain. The mechanics of bending will largely control the relationship between the major strain and bend angle but is expected to have some deviations due to the complexities of plastic bending and material behaviour such as hardening rate. We propose an expression to normalize the measured major strain from the DIC (Eq.3a) using the maximum normal strain based on the punch geometry (Eq.3b) using the formula from [11].

$$\varepsilon_{1}^{*} = \frac{\varepsilon_{1}^{DIC}}{\varepsilon_{1}^{max}} \quad \text{where} \quad \varepsilon_{1}^{max} = \ln \left(\frac{R_{outer}}{R_{Neutral}} \right) \approx \frac{1}{2} \ln(1 + t_{o} / R_{punch}) \quad \text{hence} \quad \varepsilon_{1}^{*} = \frac{\varepsilon_{1}^{DIC}}{\varepsilon_{1}^{max}} = \frac{2\varepsilon_{1}^{DIC}}{\ln(1 + t_{o} / R_{punch})} \quad (3a,b,c)$$

For simplicity, the inner bend radius is approximated by the punch tip radius which will be reasonable for moderate to large bend angles provided there is no lift-off from the punch. Thinning is also assumed to be negligible but will occur to some extent at larger bend angles. The normalized major strain, ε_1^* , is used to determine a correlation with the bend angle (Figure 11) and can then be generalized to obtain a relationship between the failure strain and bend angle for different sheet thicknesses with a constant VDA punch tip radius of 0.43 mm. This is an important feature of the correlation as the VDA bend angle will be a function of the bending severity, t/R, as the material plane strain fracture limit is a material constant. The more severe the bending, the higher the strain gradient thus the major fracture strain will be reached at a lower bend angle. Overall, the correlation with the major true strain and bend angle for the different sheet materials is promising and future work will

doi:10.1088/1742-6596/896/1/012075

consider a larger range of materials with more aluminium alloys as well as thicker materials and alternate punch tip radii.

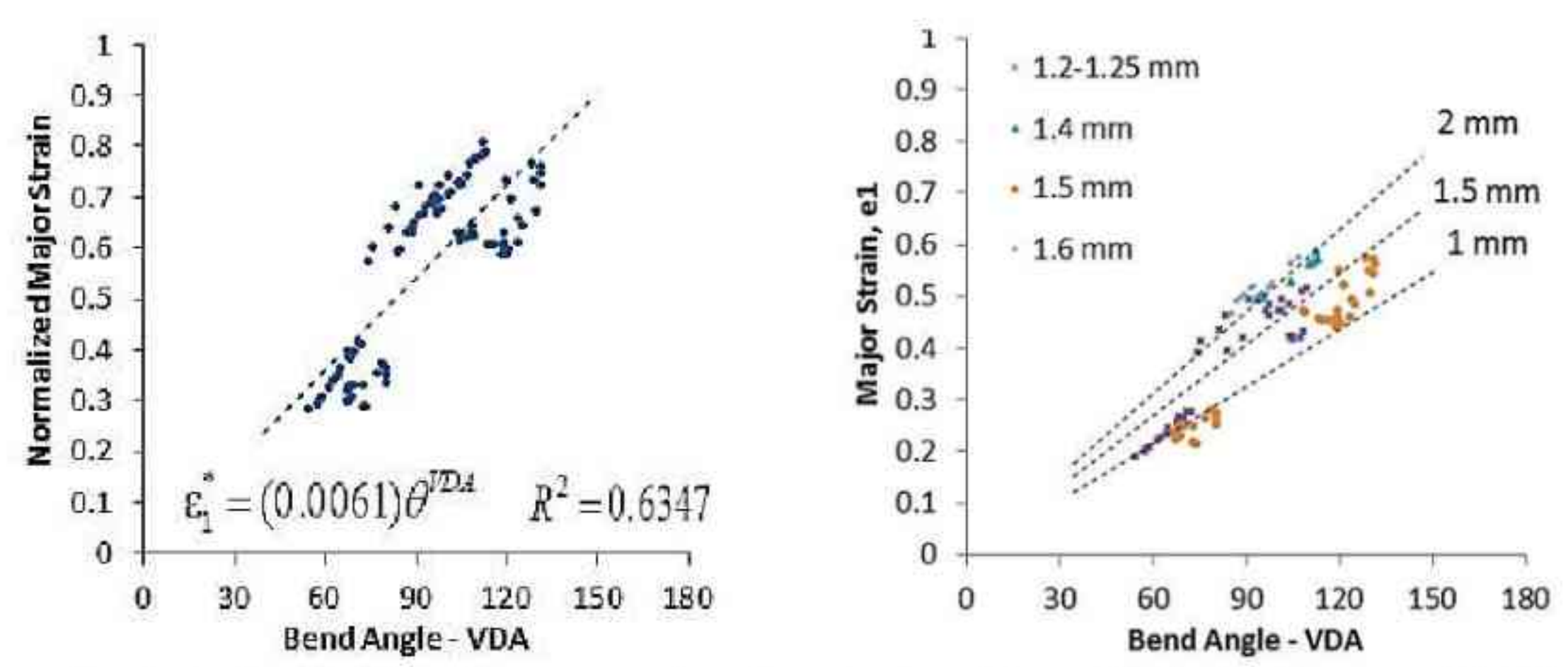


Fig. 11 Normalized strain (Left) and measured major strain with multiple thicknesses (right). The trend lines at right correspond to the relationship between the bend angle and major strain for different sheet thicknesses

6. Conclusion

A novel test frame was designed to enable the use of DIC strain measurement in a VDA 238-100 tight radius bending test. It was observed that the fracture limit threshold of the VDA standard provides a reasonable estimate for the onset of cracking from a comparison of the DIC images corresponding to the onset of micro- and macro-cracking. The VDA correlation for bend angle was also observed to be very accurate and performed slightly better than the corresponding correlation from the ISO 7438 bending standard. An algorithm was proposed to measure the bend angle using the DIC displacement data but additional refinement is required. The VDA bend angle correlation is preferable for convenience and standardization of the test results. Finally, a correlation was developed using 17 different material conditions to relate the VDA bend angle with the major strain that accounted for the sheet thickness and punch tip radius. The initial correlation results are encouraging and a larger study is required to refine and evaluate the suitability of the correlation.

References

- [1] D. Morales-Palma et al, "Assessment of the effect of the through-thickness strain/stress gradient on the formability of stretch-bend metal sheets," Materials & Design, vol. 50, pp. 798–809, 2013.
- [2] M. R. Tharrett and T. B. Stoughton, "Stretch-Bend Forming Limits of 1008 AK Steel," SAE Technical Paper Series, Mar. 2003.
- [3] VDA 238-100 test specification draft: Platebending test for metallic materials. 12/2010
- [4] P. Reu, "Virtual Strain Gage Size Study," The Art and Application of DIC, 2015
- [5] K. Omer et al, "Development of a hot stamped channel section with axially tailored properties experiments and models," International Journal of Material Forming, 2017.
- [6] P. Larour et al, "Bending Angle Calculation In the Instrumented Three-Point Bending Test," IDDRG, 2012
- [7] ISO7438(2005): Metallic materials-Bend test.
- [8] P. Larour *et al*, "Sensitivity analysis on the calculated bending angle in the instrumented bending test," *IDDRG*, 2013.
- [9] J. L. Devore, Probability and statistics for engineering and the sciences. Belmont, CA: Thomson-Brooks/Cole, 2004.
- [10] R. Neuhaus and M. Borsutzki, "Plättchen-Biegeversuch nach VDA 238-100*," Materials Testing, vol. 55, no. 9, pp. 654–659, Feb. 2013.
- [11] C. Wang et al, "Mathematical modeling of plane-strain bending of sheet and plate," Journal of Materials Processing Technology, vol. 39, no. 3-4, pp. 279–304, 1993.